PAPER

Check for updates

Unveiling CO$_2$ reactivity with data-driven methods†

Maike Eckhoff, [iD] Kerstin L. Bublitz [iD] and Jonny Proppe [iD] *

Carbon dioxide is a versatile C1 building block in organic synthesis. Understanding its reactivity is crucial for predicting reaction outcomes and identifying suitable substrates for the creation of value-added chemicals and drugs. A recent study [Li *et al.*, *J. Am. Chem. Soc.*, 2020, **142**, 8383] estimated the reactivity of CO$_2$ in the form of Mayr's electrophilicity parameter E on the basis of a single carboxylation reaction. The disagreement between experiment ($E = -16.3$) and computation ($E = -11.4$) corresponds to a deviation of up to ten orders of magnitude in bimolecular rate constants of carboxylation reactions according to the Mayr–Patz equation, $\log k = s_N(E + N)$. Here, we introduce a data-driven approach incorporating supervised learning, quantum chemistry, and uncertainty quantification to resolve this discrepancy. The dataset used for reducing the uncertainty in $E(CO_2)$ represents 15 carboxylation reactions in DMSO. However, experimental data is only available for one of these reactions. To ensure reliable predictions, we selected a training set composed of this and 19 additional reactions comprising heteroallenes other than CO$_2$ for which experimental data is available. With the new data-driven protocol, we can narrow down the electrophilicity of carbon dioxide to $E(CO_2) = -14.6(5)$ with 95% confidence, and suggest an electrophile-specific sensitivity parameter $s_E(CO_2) = 0.81(6)$, resulting in an extended reactivity equation, $\log k = s_E s_N(E + N)$ [Mayr, *Tetrahedron*, 2015, **71**, 5095].

1 Introduction

Carbon dioxide, as an abundant waste product, is a desirable C1 building block in organic synthesis.[1–5] There are two chemical recycling paths for CO$_2$ with different foci, the energy pathway and the functionalisation pathway. The former represents the reduction of CO$_2$ up to methane and enables energy storage and conversion to potential fuel substitutes.[6]

Functionalisation through carboxylation and further derivatisation, on the other hand, creates value-added chemicals and is the pathway relevant to this study. For instance, carboxylic acids transformed into esters and amides are key components in pharmaceuticals, particularly in prodrugs, which can be activated through biotransformation into active drugs.[7] Furthermore, CO$_2$ can be fixated into carbamates, which serve as key building blocks not only in pharmaceuticals but also in agricultural chemicals.[8]

TU Braunschweig, Institute of Physical and Theoretical Chemistry, Gauss Str 17, 38106 Braunschweig, Germany. E-mail: j.proppe@tu-braunschweig.de

† Electronic supplementary information (ESI) available: Information on benchmarks for computational methods, comparison between isolated reactants and pre-reaction complexes, information on conformer ensembles, information on the training and validation of regression models, overview of tested model parameters, results for the determination of the electrophilicity of electrophiles **E1**, **E2**, and **E3**, additional information on the determination of the electrophilicity of carbon dioxide, example input structures, optimised structures, interactive notebook for (reproductive) data analyses (see also https://git.rz.tu-bs.de/proppe-group/co2_electrophilicity). See DOI: https://doi.org/10.1039/d5dd00020c

Given the environmental impact of CO$_2$ as a greenhouse gas in the Earth's atmosphere, the topic of CO$_2$-binding has become increasingly important. In this context, carbamates again play a crucial role. Successful direct CO$_2$-binding from the air as carbamates as well as by metal–organic frameworks has already been demonstrated.[9–12]

Carboxylation reactions initiated by C–H activation are particularly relevant due to their high step and atom economy as well as versatility in constructing complex molecules from simple precursors.[13,14] There are various strategies for C–H functionalisation with CO$_2$, including catalysis by transition metal complexes or enzymes and mediation by Lewis acids or Brønsted bases.[14]

A frequent and prominent approach in C–H carboxylation is transition metal catalysis, where the nucleophile is activated for a subsequent reaction with CO$_2$. Metal-N-heterocyclic carbene complexes, *e.g.* with Cu(I) and Au(I), have proven to be successful catalysts for carboxylation reactions with aromatic heterocycles.[15,16] 1,2,3-Triazol-5-ylidene copper complexes were also shown to catalyse these reactions effectively.[17]

Of particular interest are base-mediated carboxylations as these can be carried out under mild and transition-metal-free conditions and are therefore more environmentally friendly and potentially more economical.[18] Reactions promoted by Cs$_2$CO$_3$ have been reported for electron-deficient aromatic heterocycles by Vechorkin *et al.*[19] Fenner and Ackermann showed that these reactions are possible under even milder conditions with KO*t*-Bu. The resulting highly nucleophilic carbanion enables the subsequent CO$_2$ insertion step at low to

moderate temperatures and atmospheric pressure of CO_2.[20] Felten *et al.* also pursued a base-mediated approach in their work on the carboxylation of azoles activated and stabilised by silyl triflate reagents.[21]

Due to their highly nucleophilic nature, N-heterocyclic carbenes (NHCs) have come into focus for CO_2 fixation in organocatalysis.[5,22] Several examples showing the ability of NHCs to bind CO_2 have been reported.[23–25]

While highly reactive nucleophiles offer significant advantages in carboxylation reactions, they also present notable drawbacks related to selectivity, stability, handling, and environmental impact. Understanding the reactivity of CO_2 is crucial for optimising reaction conditions and developing tailored nucleophiles that are milder but still reactive enough to form products with CO_2, thereby expanding the scope of CO_2-based syntheses towards late-stage functionalisation. Unveiling the reactivity of CO_2 therefore is key to creating value-added chemicals and drugs in a more sustainable and controlled manner.

One way to characterise the reactivity of CO_2 is Mayr's electrophilicity parameter E, which can be determined by calibration against a series of reference nucleophiles according to the Mayr–Patz equation,[26–28]

$$\log k = s_N(E + N) \tag{1}$$

Here, k is the bimolecular rate constant of the transformative nucleophile–electrophile encounter at 20 °C, and N and s_N represent solvent-dependent parameters for nucleophilicity and nucleophile-specific sensitivity, respectively. (Note that the logarithm of k is reported as a dimensionless number. As long as it is ensured that the reactivity parameters strictly correspond to a specific set of units—here, $[k] = \text{M}^{-1}\,\text{s}^{-1}$—this expression is unambiguous).

A recent study by Mayr, Ofial, and co-workers suggests two distinct values for E of carbon dioxide (experiment, $E = -16.3$; computation, $E = -11.4$), which encompass the values for benzaldehyde and fairly strong Michael acceptors.[29] This gap represents a deviation of about five orders of magnitude in bimolecular rate constants of carboxylation reactions if s_N is close to one, a discrepancy that is clearly too pronounced to enable reasonable estimates of the rate and selectivity of carboxylation reactions. Both $E(CO_2)$-values were derived from a single identical reaction, *i.e.* the carboxylation of the indenide anion,

$$E(CO_2) = \frac{\log k(CO_2 + \text{indenide})}{s_N(\text{indenide})} - N(\text{indenide}) \tag{2}$$

Hence, no error compensation by calibrating $E(CO_2)$ against several nucleophiles was possible. (Note that the Gibbs free energy of activation obtained from IEFPCM(DMSO)/B3LYP-D3/6-311+G(d,p) calculations, which corresponds to $E = -14.0$, was subjected to a statistical correction to align it with the results obtained for heteroallenes other than CO_2; see Table 4 and Fig. 13 in Li *et al.*[29])

Nicoletti *et al.*[30] calculated $E(CO_2)$ for four additional reactions by using adopted versions of eqn (2), suggesting a range of lower reactivity ($-18.7 < E(CO_2) < -15.3$). No calibration of E was
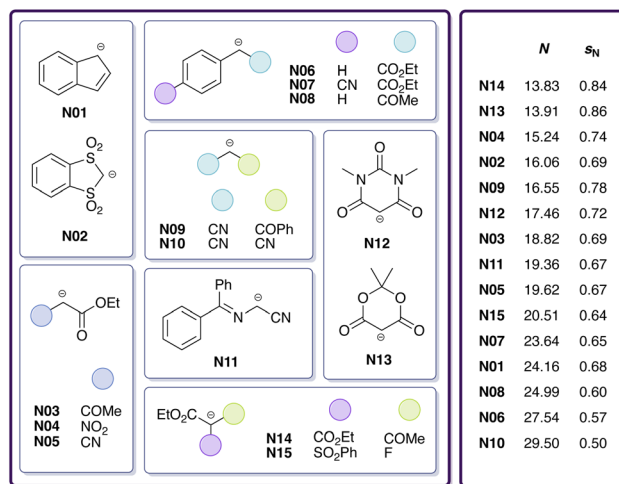

Fig. 1 Carbanions (15 in total) considered in this study for reactions with CO_2 in DMSO, including identifiers and reactivity parameters (N, s_N).

applied. Instead, every nucleophile was linked to an individual value of E for carbon dioxide, an issue to be avoided in the construction of a global reactivity scale. An alternative approach was taken by Liu *et al.*,[31] who created a machine-learning-based web prediction tool trained on experimental E parameters from Mayr's Database of Reactivity Parameters,[32,33] placing the electrophilicity value of CO_2 at $E = -15.02$ without providing a species-specific error estimate. Another web prediction tool based on methyl anion affinities (correlated to E) and methyl cation affinities (correlated to N) created by Ree *et al.* includes error estimates for specific electrophilic and nucleophilic sites.[34,35] A direct estimation of Mayr's reactivity parameters, however, is not possible with this tool.

The goal of this work is to reduce the aforementioned uncertainty in CO_2 reactivity by narrowing down the range of $E(CO_2)$. For this purpose, we investigate reactions of CO_2 with 15 carbanions (Fig. 1) in DMSO by means of quantum chemical calculations involving transition state searches to obtain estimates of $\log k$. These carbanions have been selected from Mayr's database and span a wide nucleophilicity range. However, for only one of these reactions (CO_2 + indenide anion **N01**) experimental data is available. To assess the validity of different quantum chemical methods, we benchmark calculated rate constants against experimental reference values for this and six similar reactions involving the chemically related heteroallene carbon disulphide.[29] To improve the quality of calculated rate constants, we train a multivariate linear (ML) model on these seven and 13 additional heteroallene–carbanion reactions for which experimental data is available (also from Li *et al.*[29]). Finally, by combining least-squares optimisation with Bayesian bootstrapping,[36,37] we quantify E by calibration against ML-derived $\log k$ values.

2 Methods

2.1 Quantum chemical protocol

We took the experimental protocol applied by Li *et al.*[29] into account, which is adapted from work by Fenner and

Ackermann.[20] The reaction is transition-metal-free and carried out under mild conditions, namely at 20 °C and atmospheric pressure. After deprotonation of a carbon-centred nucleophile with KOt-Bu, the carbanion formed reacts with CO_2, which was previously dissolved in DMSO.

2.1.1 Conformational search and structure optimisation. CREST (version 2.12)[38,39] was employed to find all conformers of each molecule (CO_2, nucleophile, nucleophile–CO_2 transition state) using GFN2-xTB.[40] Full structure optimisations were then carried out on every conformer with Gaussian (version 16, revision C01)[41] using the hybrid exchange–correlation functional B3LYP,[42,43] D3-type dispersion corrections with Becke–Johnson damping[44,45] (D3(BJ)), and the def2-SVPD basis set.[46–48] The latter was generated with the Basis Set Exchange program[49] and added manually for the Gaussian calculations. The diffuse basis functions contained in the basis set (therefore the terminal character "D") are essential to properly model the electronic structure of the carbanionic site. Preliminary tests motivating the choice of basis set are given in Section S1.† For verifying converged structures, harmonic frequency calculations were performed for all species with the same settings. Goodvibes[50] was employed to apply the quasi-harmonic correction to the vibrational entropy[51] computed by Gaussian. The procedure outlined here was also applied to van-der-Waals pre-reaction complexes, which are neglected in this study as they were found to be generally less stable than the corresponding isolated reactants (see Section S2† for more details).

2.1.2 Transition state search. To obtain reasonable starting structures for transition state optimisations, restricted Gaussian scans were performed based on the optimised CO_2–nucleophile adducts. The dissociation of the CO_2–carbanion coordinate was scanned in 999 steps with a stepsize of 0.001. Two different types of algorithms implemented in Gaussian were employed for the transition state search: the QST3 algorithm[52] and the Berny algorithm without eigenvector following.[53] After successful optimisation of the transition state, a constrained CREST calculation was applied while keeping the CO_2–carbanion distance fixed to obtain a conformer ensemble of the transition state. The distance was set to the length of the distance in the already found transition state. For verifying converged transition state optimisations, intrinsic reaction paths were calculated and the presence of a single imaginary mode was checked.

2.1.3 Implicit solvation modelling. Single-point calculations including implicit solvation (SMD model[54]) for DMSO were executed. B3LYP-D3(BJ) was employed together with the def2-TZVPD basis set[46–48] as tests have shown an energetic improvement over def2-SVPD for the specific case studied here (details in Section S1†). Finally, the lowest-energy conformer was determined for each species and transition state. These lowest-energy conformers were used to calculate Gibbs free energies of activation and rate constants. An overview of conformer ensemble statistics is given in Section S3.†

2.1.4 Towards higher accuracy: DLPNO-based electronic-energy corrections. Additional single-point calculations were carried out with ORCA (version 5.0.3)[55,56] for a subset of reactions to improve upon the electronic energy without changing the structure of the species. The first additional method involves the hybrid functional B2PLYP[57] in combination with the DLPNO approximation for MP2,[58] the def2-TZVPD basis set and D3(BJ) dispersion corrections. The second additional method involves DLPNO-CCSD(T)[59,60] calculations in combination with the aug-cc-pVnZ basis sets ($n = T, Q$)[61,62] and aug-cc-pVmZ auxiliary basis sets ($m = Q, 5$).[63,64] The DLPNO-CCSD(T) energies were extrapolated to the complete-basis-set (CBS) limit with the extrapolation scheme developed by Halkier et al.[65,66] The Hartree–Fock (HF) and correlation (corr) parts of the electronic energy were separately extrapolated according to the following scheme,

$$E_{el}^{CBS} \approx \frac{E_{el}^{HF/QZ}\exp\{1.63X\} - E_{el}^{HF/TZ}\{\exp 1.63(X - 1)\}}{\exp\{1.63X\} - \exp\{1.63(X - 1)\}}$$

$$+ \frac{E_{el}^{corr/QZ}X^3 - E_{el}^{corr/TZ}(X - 1)^3}{X^3 - (X - 1)^3}. \quad (3)$$

In the aforementioned expression, X is the cardinal number of the larger basis set (here, $X = 4$). In Table 1, abbreviations are introduced for the different computational settings applied in this work.

2.2 Data-driven protocol

All data analysis tools presented in this section can be accessed through the project-related GitLab repository.[67]

2.2.1 Multivariate linear (ML) model. After standardising the data, Bayesian Multivariate Linear (ML) regression with Automatic Relevance Determination (ARD)[68] was performed (cf. eqn (7)) using Scikit-learn 1.5.1.[69] Default parameters for ARD regression were applied, except for the following, which were set to specified values: `tol` = 10^{-6}, `lambda_2` = 0.003, `alpha_2` = 0.27, and `alpha_1` = 3.0. These parameters were refined through an extensive grid search, with success determined by the highest cross-validation score. To validate the resulting model, a leave-one-out approach was employed: with $n = 20$ reactions in the dataset, $n - 1$ data points were used to train n models. The left-out reaction was used for evaluating the model's performance.

2.2.2 Calibration of E and (s_E). We considered two calibration problems. In the first problem, $\log k = s_N(E + N)$ and only E is determined. In the second problem, $\log k = s_E s_N(E + N)$ and both E and s_E are determined. The least-squares method was applied to calibrate these electrophile-specific parameters against n reactions for which experimental rate constants are available,

Table 1 Computational settings selected for Gibbs free energy calculations and their abbreviations used in this work. All energy calculations are based on B3LYP-D3(BJ)/def2-SVPD-optimised structures

Abbreviation	Computational setting for the energy
B3LYP	B3LYP-D3(BJ)/def2-TZVPD/SMD(DMSO)
DLPNO-B2PLYP	DLPNO-B2PLYP-D3(BJ)/def2-TZVPD/SMD(DMSO)
DLPNO-CCSD(T)	DLPNO-CCSD(T)/CBS/SMD(DMSO)

$$E^{opt}, s_E^{opt} = \arg\min_{E, s_E} \sum_{i=1}^{n} \left[\log k_{exp,i} - \log k_{ML,i}(E, s_E) \right]^2 \quad (4)$$

Optimisation of these nonlinear calibration problems was performed using the basin-hopping method[70] implemented in SciPy 1.10.1.[71]

2.2.3 Uncertainty quantification of E (and s_E). To obtain distributions of E (and s_E) from which uncertainties can be derived, we applied Bayesian bootstrapping[36,37] to the least-squares calibration problem. From the dataset at hand, B new datasets, so-called bootstrap samples, were generated. Each sample was labeled by an index b, and for each of these samples the calibration equation was formulated,

$$E^{opt,(b)}, s_E^{opt,(b)} = \arg\min_{E, s_E} \sum_{i=1}^{n} p_i^{(b)} \left[\log k_{exp,i} - \log k_{ML,i}(E, s_E) \right]^2$$

$$(5)$$

The weight $p_i^{(b)}$ can take any value between zero and one under the constraint that $\sum_{i=1}^{n} p_i^{(b)} = 1$. Since every bootstrap sample is represented by a unique set of weights, the optimal reactivity parameters were slightly different for each set, hence the designations $E^{opt,(b)}$ and $s_E^{opt,(b)}$.

We chose $B = 1000$ for this study. The optimal values for E and s_E were estimated as medians (50th percentiles) of their respective B bootstrapped values. To estimate the probability P that E or s_E are located within a certain range of values, we calculated both the $[(1-P)/2]$th and the $[(1+P)/2]$th percentiles, which define the lower and upper bounds of the corresponding confidence interval. For instance, for a 95% confidence interval, $P = 0.95$, $[(1-P)/2] = 0.025$, and $[(1+P)/2] = 0.975$.

3 Results and discussion

3.1 Assessment of quantum chemical methods

Prior to determining the electrophilicity of CO_2, we benchmarked different electronic-structure methods of varying sophistication (based on B3LYP, DLPNO-B2PLYP, DLPNO-CCSD(T); see Section 2.1.4 and Table 1) against the experimental rate constants listed in Table S10.† Since there is only a single experimental rate constant available for the reaction of CO_2 with a nucleophile (**N01**) from Mayr's database, we included six additional experimental rate constants for reactions of the chemically related carbon disulphide (**E1**)[29] with carbanions (**N01, N07, N16, N17, N18, N19**; see Fig. 2) in DMSO.

In Table 2, the root mean square error (RMSE) and maximum absolute error (max. AE) are shown for the Gibbs free activation energy $\Delta G_{sol}^{\ddagger}$ and $\log k$ in comparison to the experimental results. All values correspond to a temperature of 20 °C. The RMSE values are smallest for DLPNO-CCSD(T). However, the max. AE is largest for DLPNO-CCSD(T) but smallest for B3LYP. When including the reaction of CO_2 with **N01**, both RMSE and max. AE are smallest for B3LYP. Since all results in Table 2 are based on B3LYP-optimised structures, the assumption that the reactants and the transition states are structurally similar across the different electronic-
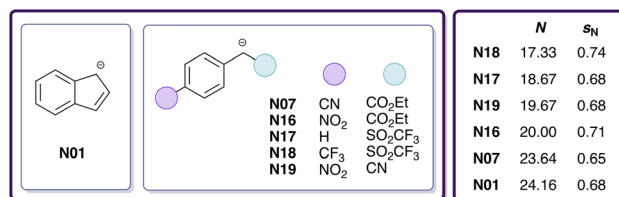

Fig. 2 Carbanions involved in reactions with E1 (CS_2) in DMSO, including identifiers and reactivity parameters (N, s_N), for which experimental $\log k$ values were determined.[29]

Table 2 RMSE and maximum absolute error (max. AE) in $\Delta G_{sol}^{\ddagger}$ (kcal mol^{-1}) and $\log k$ for different quantum chemical approximations applied to reactions of **E1** (CS_2) with six carbanions in DMSO in comparison to experimental data. Statistics including the reaction of CO_2 with the indenide anion **N01** in DMSO are given in parentheses. See also Table S10

	B3LYP	DLPNO-B2PLYP	DLPNO-CCSD(T)
RMSE $\Delta G_{sol}^{\ddagger}$	2.44 (2.26)	2.60 (2.47)	2.22 (2.47)
max. AE $\Delta G_{sol}^{\ddagger}$	3.25	3.71	4.12
RMSE $\log k$	1.82 (1.68)	1.94 (1.84)	1.65 (1.84)
max. AE $\log k$	2.42	2.77	3.07

structure methods could be critical for explaining the increasing max. AE in DLPNO-B2PLYP and DLPNO-CCSD(T) in comparison to B3LYP.

As the average error in $\log k$ is comparable among the different electronic-structure approximations, B3LYP appears to be a reasonable choice given its relatively low computational cost. However, the scatter of residuals ($\log k_{exp} - \log k_{B3LYP}$) is too high for a proper quantification of electrophilicity, and the limited number of reaction data is insufficient to apply statistical corrections.

To enhance our analysis, we included 15 additional experimental rate constants for reactions carried out in DMSO involving other heteroallenes (Fig. 3a) and carbanions (Fig. 3b).[29] For these additional heteroallene–carbanion reactions, we followed the same computational protocol as before (see Section 2.1) but omitted further DLPNO-B2PLYP and DLPNO-CCSD(T) calculations. The reactions **E4-N07** and **E4-N20** were excluded due to the excessive size of their transition state conformer ensembles (see Section S3†), leading to 20 modelled reactions in total (Table 3). Table 4 shows the updated RMSE and max. AE for the Gibbs free activation energy $\Delta G_{sol}^{\ddagger}$ and $\log k$ in comparison to the experimental results for this set of reactions. Both RMSE and max. AE decrease compared to the previous values (Table 2). However, the $\log k$ values from our DFT calculations still do not align well with the experimental results. To improve the accuracy of $\log k$ predictions and, hence, ensure a reliable quantification of the electrophilicity of CO_2, we next investigated how statistical corrections can be incorporated into the workflow.

3.2 Improving upon quantum chemical $\log k$ values

To approximate $\log k_{exp}$ of heteroallene–carbanion reactions over a wide range of reactivity, suitable parameters must be
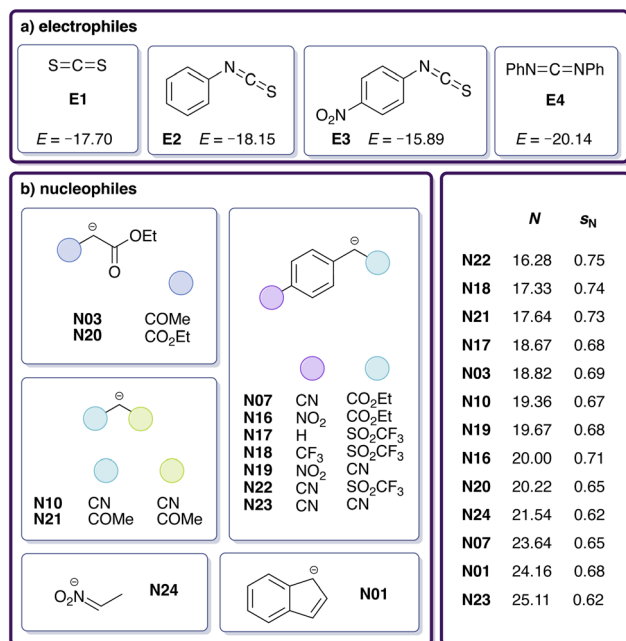
Fig. 3 Dataset of (a) electrophiles and (b) nucleophiles involved in reactions with available experimental rate constants measured in DMSO,[29] including identifiers and reactivity parameters (E, N, s_N).

Table 3 Gibbs free energy of activation $\Delta G_{sol}^{\ddagger}$ and rate constants derived from quantum chemical calculations ($\log k_{QC}$) compared to their experimental values[29] ($\log k_{exp}$) for each nucleophile–electrophile reaction of the ML training set. Reference IDs[29] are listed in Table S5

Elec.	Nuc.	$\Delta G_{sol}^{\ddagger}$ [kcal mol^{-1}]	$\log k_{QC}$	$\log k_{exp}$ [29]
E1	**N01**	10.25	5.14	4.99
	N07	10.32	5.09	3.25
	N16	12.28	3.63	1.34
	N17	12.81	3.24	1.00
	N18	14.41	2.04	−0.38
	N19	14.50	1.98	1.42
E2	**N03**	17.36	−0.16	0.06
	N10	18.23	−0.80	1.43
	N17	15.29	1.38	0.31
	N21	18.40	−0.93	−0.19
	N24	12.77	3.26	1.72
E3	**N03**	14.68	1.84	1.96
	N10	15.17	1.48	3.09
	N20	12.54	3.44	2.43
	N21	14.78	1.77	0.88
	N22	15.20	1.45	0.39
E4	**N03**	19.11	−0.62	−1.46
	N17	16.20	0.71	−0.55
	N23	14.07	2.30	2.23
CO₂	**N01**	10.20	5.18	5.32

identified. Different sets of parameters were tested for this purpose: (a) individual contributions to the Gibbs free activation energy $\Delta G_{sol}^{\ddagger}$ (details in Section 2 of ref. 72), (b) molecular descriptors from conceptual DFT based on recent studies,[73–76] and (c) Mayr's nucleophile-specific reactivity parameters s_N and

Table 4 RMSE and maximum absolute error (max. AE) in $\Delta G_{sol}^{\ddagger}$ (kcal mol^{-1}) and rate constants ($\log k_{QC}$) obtained from quantum chemical calculations for 19 reactions of heteroallenes with carbanions in DMSO in comparison to experimental data. Statistics including the reaction of CO_2 with the indenide anion **N01** in DMSO are given in parentheses. See also Table 3

	$\Delta G_{sol}^{\ddagger}$	$\log k_{QC}$
RMSE	1.87 (1.82)	1.39 (1.36)
max. AE	3.25	2.42

N. Section S4† provides a summary of all tested parameters, which are also listed in Table S7†, together with detailed information on their selection (see also Table S6†) and leave-one-out validations (Fig. S2–S22†).

Bayesian regression with Automatic Relevance Determination (ARD)[68] was performed after preprocessing the data (see Section 2.2.1 for more details). In total, 20 models were trained per examined combination of parameters, excluding each reaction once from the training dataset. With this leave-one-out approach, we attempted to mitigate the effect of overfitting in order to reliably assess $\log k$ predictions for CO_2–nucleophile reactions not included in the training set.

The best working combination of parameters includes, from group (a), the temperature-scaled entropy of the nucleophile, TS_{nuc}, from group (b), the electronic chemical potential[77,78] of the electrophile, defined as

$$\mu_{elec} = \frac{\varepsilon_{elec}^{HOMO} + \varepsilon_{elec}^{LUMO}}{2} \quad (6)$$

and, from group (c), Mayr's nucleophilicity N. The final ML model equation is given by

$$\log k_{ML} := w_0 + w_1 TS_{nuc} + w_2 \mu_{elec} + w_3 N \approx \log k_{exp} \quad (7)$$

In Table 5, the model coefficients w_0 to w_3 are listed for the final multivariate linear (ML) model including all 20 reference reactions. RMSE and max. AE of the corresponding $\log k_{ML}$ values (Table 6) are about four times smaller compared to those obtained from Gibbs free energies of activation ($\log k_{QC}$). This finding indicates that a statistical model combining quantum chemical (TS_{nuc} and μ_{elec}) and empirical (N) information systematically outperforms DFT-based thermochemistry. In fact, not a single parameter combination from group (a) alone could achieve an accuracy similar to that of the best combination shown in eqn (7).

Table 5 Coefficients w_0 to w_3 of the final ML model shown in eqn (7). The coefficients are dimensionless as we used standardized values

Coefficient	Term	Value
w_0	—	+1.5042
w_1	TS_{nuc}	−0.4399
w_2	μ_{elec}	−0.8825
w_3	N	+1.1256

Table 6 RMSE and maximum absolute error (max. AE) in calculated rate constants (log k) for 19 reactions of non-CO_2 heteroallenes with carbanions in DMSO (Table 3) in comparison to experimental data. Statistics for the ML model refer to leave-one-out errors

	log k_{QC}	log k_{ML}
RMSE	1.39	0.35
max. AE	2.42	0.58

Fig. 4 shows a leave-one-out plot of the log k_{QC} values (unfilled circles) and the log k_{ML} values (filled circles) *versus* their experimental analogues for the 20 reference reactions. The prediction of the reaction left out of training in this case, CO_2–**N01**, is shown in red. Results for the 19 other leave-one-out models and the final ML model are provided in Section S4.†

To examine whether this approach is transferable to reactions of CO_2 with nucleophiles not included in the training of the ML model, we simulated analogous scenarios, two for each of the other heteroallenes **E1**–**E3**, respectively. In each of the six simulations, the ML model was retrained using data from only one reaction of the selected heteroallene with a nucleophile that is also involved in at least one other reaction (see Section S5†). (In the original ML model, CO_2 is the heteroallene for which experimental data with only one nucleophile, **N01**, is available, which is also present in a reaction with **E1**). In all cases, the agreement between experimental and ML-predicted log k values for reactions with the underrepresented heteroallene is high, although several nucleophiles are excluded from the respective model trainings. These results indicate that the ML model is transferable to reactions with other heteroallenes as well as other carbanions, an essential prerequisite for predicting the kinetics of yet-unobserved carboxylation reactions.

In addition to delivering more accurate results, the ML model provides computational cost advantages over conventional quantum chemical calculations. The most significant computational time is required for the transition state search in the latter case. The proposed ML model effectively circumvents this time-intensive process.
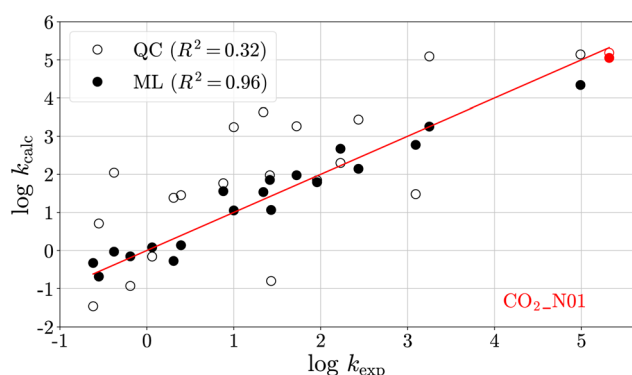

Fig. 4 Rate constants (log k) from quantum chemical (QC) calculations (unfilled circles) and those obtained from multivariate linear (ML) regression (filled circles) *versus* their experimental analogues for the heteroallene–carbanion reactions listed in Table 3. The reaction shown in red has been left out for training and is predicted by the ML model.

3.3 Determination of E(**E1**): experiment *vs.* computation

To validate the ML model, we assess the reproducibility of E of **E1** (CS_2), whose experimental value is reliably known ($E = -17.7$). For this purpose, we compare the calibration of E against log k_{exp} (Fig. 5a and Table 7) with that against log k_{ML} (Fig. 5b and Table 7). The sampled distributions of experimental and ML-derived E values obtained from Bayesian bootstrapping[36,37] are strongly overlapping (Fig. 5c), and the ML-predicted value ($E = -17.6$) is very close to its experimental reference, especially when taking into account that the resulting deviation in log k is much smaller than the uncertainty in log k introduced by the Mayr–Patz approach.[36]

The close agreement is not particularly surprising as the corresponding reactions are part of the training set for the ML model (eqn (7)). The same holds for the calibration of E of **E2** and **E3**, the results of which are provided in Section S5.† However, we obtain similar results (Tables S11–S13†) when the ML-predictions of the six data-sparse simulations mentioned in the previous section are employed, where only one of the experimentally investigated reactions is part of the training procedure.

3.4 Determination of E(CO_2)

To quantify the electrophilicity parameter E for carbon dioxide, we applied the same calibration procedure as in the previous section. Due to the availability of only one experimental data point, we calibrated E(CO_2) against log k_{ML} (Table S14†) predicted for 15 carboxylation reactions with different carbanions (Fig. 1 and Table S9†) in DMSO; see Fig. 6-1a.

The resulting distribution of E(CO_2) (Fig. 6-1b and Table 8) has a median of $E = -15.45$ and a two-sided 95% confidence interval of $-16.00 < E < -14.97$. This median along with its confidence interval lies between the two values determined by Li *et al.*[29] (experiment, $E = -16.3$; computation, $E = -11.4$), which are both based on a single reaction (with the indenide anion **N01**). In direct comparison to the single experimental reference, the reactivity of CO_2 increases from -16.3 to -15.5.

However, as evident in Fig. 6-1a, a noticeable systematic deviation exists in the ML data (filled circles). At lower N values, the data points are positioned above the median, while as N increases, the data points generally lie below the median line. A possibility to examine the underlying data for signs of autocorrelation, which may indicate systematic errors, is the Durbin–Watson test, a statistical test used to assess the independence of residuals, z_{ij}, in regression analysis[79,80]

$$d = \frac{\sum (\Delta z_{ij})^2}{\sum z_{ij}^2} \quad (8)$$

with $0 < d < 4$ and no autocorrelation present when $d = 2$. The test result, $d = 0.47$, confirms the observation of systematic deviations in the data.

One assumption in the Mayr–Patz equation (eqn (1)) is that the electrophile-specific sensitivity parameter s_E equals one.[81] Mayr and coworkers have demonstrated that this assumption is valid for many different electrophiles,[27,81] including the heteroallenes **E1**–**E4**.[29] In the linear visualisation of the Mayr–Patz
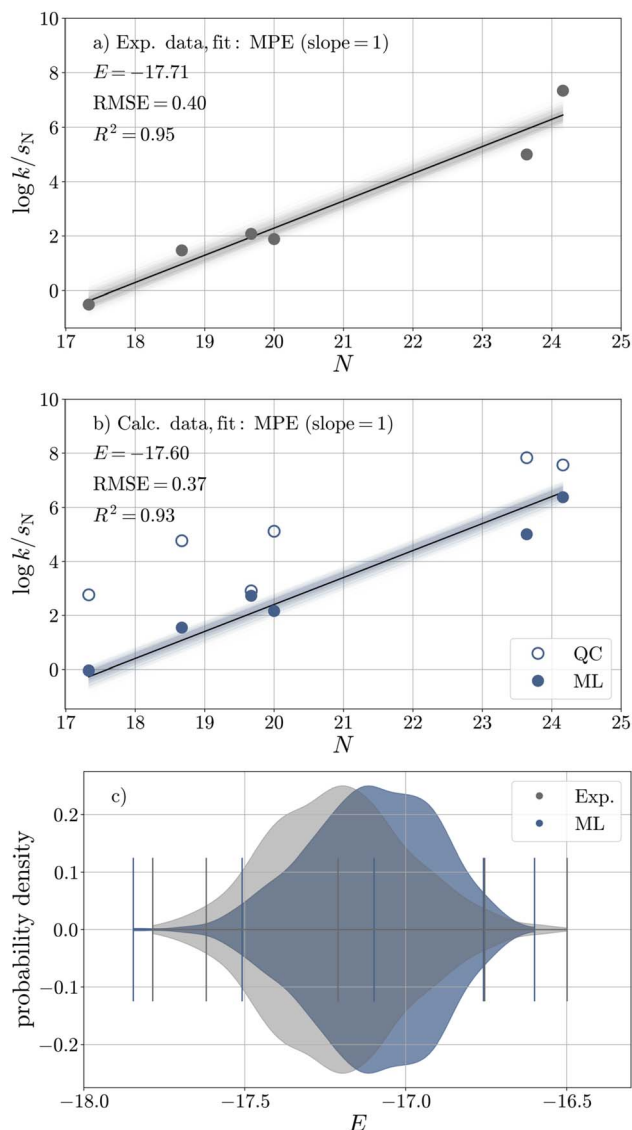
Fig. 5 Calibration of E against (a) experimental rate constants and (b) rate constants obtained from the ML model (filled circles) for six reactions of carbanions with **E1** (CS_2) in DMSO based on bootstrapped least-squares optimisation with respect to the Mayr–Patz equation (MPE, eqn (1)). The quantum chemical (QC) data is shown in unfilled circles for comparison. (c) Bootstrapped distributions of E(**E1**) based on experimental (grey) and ML (blue) data.

Table 7 Mayr's electrophilicity E for **E1** (CS_2) and performance statistics (RMSE, R^2) derived from the calibration results shown in Fig. 5. The results are based on experimental values, ML values, and QC values for comparison. See Table S11 for more details

	Exp.	ML	QC
E_{lower}	−18.12	−18.01	−16.16
E	**−17.71**	**−17.60**	−15.39
E_{upper}	−17.25	−17.26	−14.64
u_{95} (E)	0.87	0.75	1.51
RMSE ($\log k$)	0.40	0.37	0.72
R^2 ($\log k$)	0.95	0.93	0.68

relationship, the slope of the plot of $\log k/s_N$ versus N equals s_E. We were curious to see if a more general equation for nucleophile–electrophile reactions that contains s_E as a free parameter,

$$\log k = s_E s_N (E + N) \tag{9}$$

yields a more accurate prediction of E and decreases the strong autocorrelation observed for $s_E = 1$.

Fig. 6-2a shows a significant improvement when applying the generalised equation over the Mayr–Patz equation, evidenced by an increase/decrease in R^2 (from 0.89 to 0.97)/RMSE (from 0.72 to 0.40) and a significant reduction in autocorrelation ($d = 1.22$). Regarding the high calibration accuracy, it is worth mentioning that only four nucleophiles (**N01, N03, N07, N10**) were included in both the ML model as well as CO_2 dataset. This result suggests that s_E should be explicitly considered as a parameter in the quantification of E for CO_2.

The resulting distribution of E(CO_2) (Fig. 6-2b and Table 8) has a median of $E = −14.62$ and a two-sided 95% confidence interval of $−15.05 < E < −14.18$. For s_E(CO_2), the resulting distribution has a median of $s_E = 0.81$ and a two-sided 95% confidence interval of $0.73 < s_E < 0.87$. These distributions allow us to estimate reaction-specific uncertainty in $\log k$ (Section S6†), which we provide in Table S16†. With a confidence of 95%, the uncertainty in rate constants of carboxylation reactions equals about one order of magnitude. It increases slightly towards both ends of the nucleophilicity range under consideration.

Building on this set of nucleophiles, we find evidence that s_E takes values significantly smaller than one (0.7–0.8, see Table S20†) also for heteroallenes **E1–E3**, indicating a more general trend. A distinctive aspect is that heteroallenes are linear in their ground state but adopt an increasingly bent structure along the reaction coordinate. This change can affect the relative stabilisation of transition states and products, both intrinsically and through solvent interactions, thereby potentially altering the sensitivity of the activation energy to changes in the reaction energy. This sensitivity coefficient, better known as the Brønsted coefficient, has been shown to be proportional to the s_N parameter in the Mayr–Patz framework.[82] Assuming an analogous relationship for the s_E parameter, the pronounced structural change in heteroallenes during nucleophilic attack may explain the deviation from the typical case where $s_E = 1$. The directional nature of nucleophilic attack on CO_2 may further contribute to this effect. Given the complexity of these influences, a detailed quantitative analysis would be required to draw firm conclusions. For now, we focus on the narrowness of the confidence intervals for E and s_E, which allows us to explore the application scope of CO_2 (and potentially other heteroallenes).

3.5 Identifying suitable substrates for CO_2

Applying the extended Mayr–Patz equation (eqn (9)), kinetically suitable nucleophiles for reactions with CO_2 can be identified. As a rule of thumb, electrophile–nucleophile reactions can be observed at room temperature (20 °C) if $\log k > −6$.[81] The diffusion limit is reached at $\log k \approx 8$, where the validity of the Mayr–Patz equation breaks.[28] To illustrate the reaction scope of
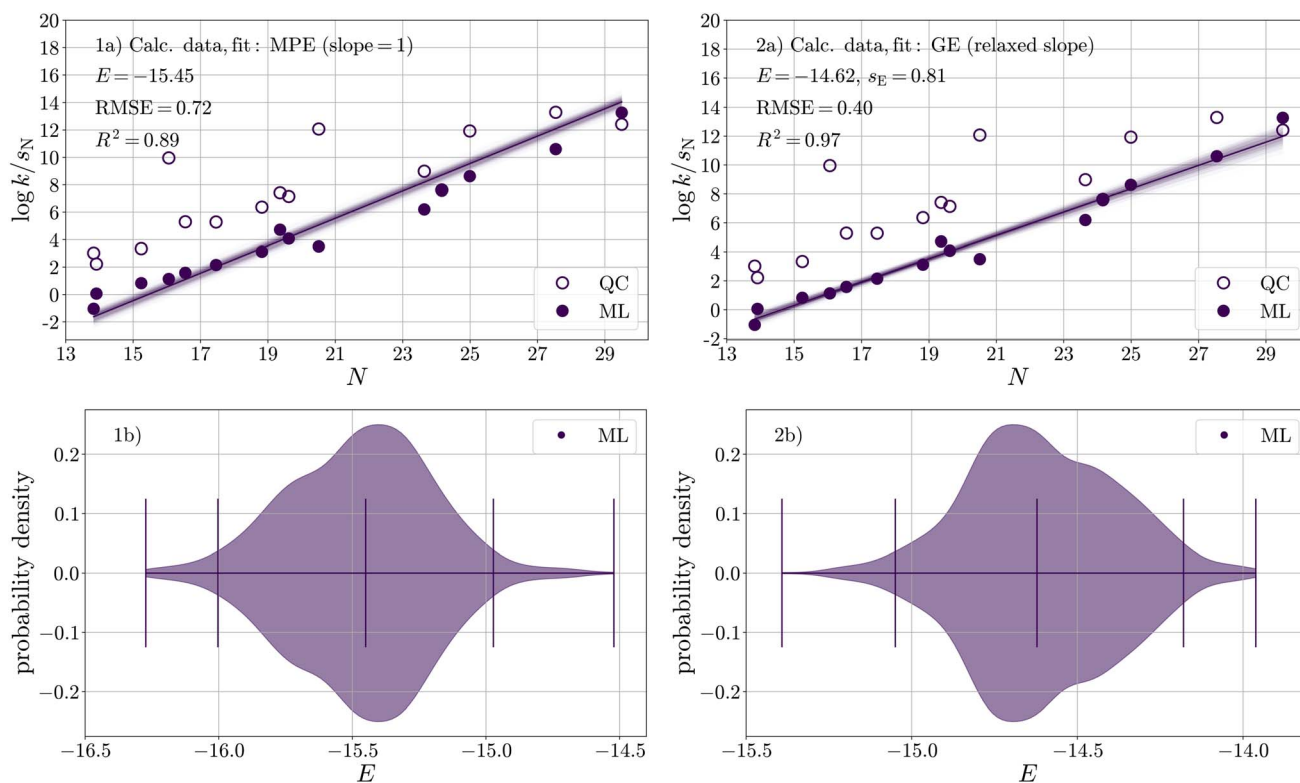
Fig. 6 (a) Calibration of E against rate constants obtained from the ML model for 15 reactions of CO_2 with carbanions in DMSO with respect to (1) the Mayr–Patz equation (MPE, fixed slope, eqn (1)) and (2) the more general equation of reactivity (GE, relaxed slope, eqn (9)). (b) Corresponding bootstrapped distributions of $E(CO_2)$.

Table 8 Mayr's electrophilicity E and s_E for CO_2 and performance statistics (RMSE, R^2) derived from the calibration results shown in Fig. 6. See Table S15 for more details

	MPE (eqn (1))	GE (eqn (9))
E_{lower}	−16.00	−15.05
E	**−15.45**	**−14.62**
E_{upper}	−14.97	−14.18
$u_{95}(E)$	1.03	0.87
$s_{E,lower}$	—	0.73
s_E	**1.00**	**0.81**
$s_{E,upper}$	—	0.87
$u_{95}(s_E)$	—	0.13
RMSE ($\log k$)	0.72	0.40
R^2 ($\log k$)	0.89	0.97

CO_2, we establish a "CO_2 reactivity cone", which is defined by two axes, N and $1/s_N$ (Fig. 7). Every nucleophile with known reactivity parameters can thus be assigned a specific position in the cone plot and falls either into the cone (reaction scope) or outside of it (unobservable or diffusion-controlled reactions). Within this cone, 229 carbon-centred nucleophiles from Mayr's database[32] have been included, emphasising some examples with low nucleophilicity values, highlighted in red. These nucleophiles are relatively mild but, according to the extended Mayr–Patz equation, reactive enough to form products with CO_2. For instance, certain cyclic α-diazo carbonyl compounds and heteroarenes (measured in DCM) fall into this category.

With a fixed s_E parameter, the cone would be narrower, shifting many of these "mild" compounds outside the cone. In this light, it is an encouraging result that $s_E < 1$, as it widens the substrate scope of carboxylation reactions.

By utilising available web prediction tools for fast predictions of N,[31,34,35] nucleophiles not yet included in Mayr's database can be accessed. However, it is important to consider the uncertainty estimates provided by these tools.

Through various approaches for the activation of nucleophiles mentioned earlier,[2,4,14] such as binding to a transition metal, but also by activating CO_2 in a Lewis–acidic medium, weaker nucleophiles can become sufficiently reactive, which significantly increases the number of suitable reaction partners for carboxylation reactions further. In case of CO_2 activation, the boundaries of the cone would shift, whereas nucleophile activation shifts substrates into and out of the cone.

4 Conclusions and outlook

We developed a computational pipeline integrating supervised learning, quantum chemistry, and uncertainty quantification to quantify the reactivity of heteroallenes (X = C=Y), most notably carbon dioxide (CO_2), in the form of Mayr's electrophilicity parameter E. Benchmarking revealed that conventional quantum chemical calculations combined with standard thermochemistry and canonical transition state theory fail to reproduce experimental rate constants of nucleophilic attack by carbanions at heteroallenes.
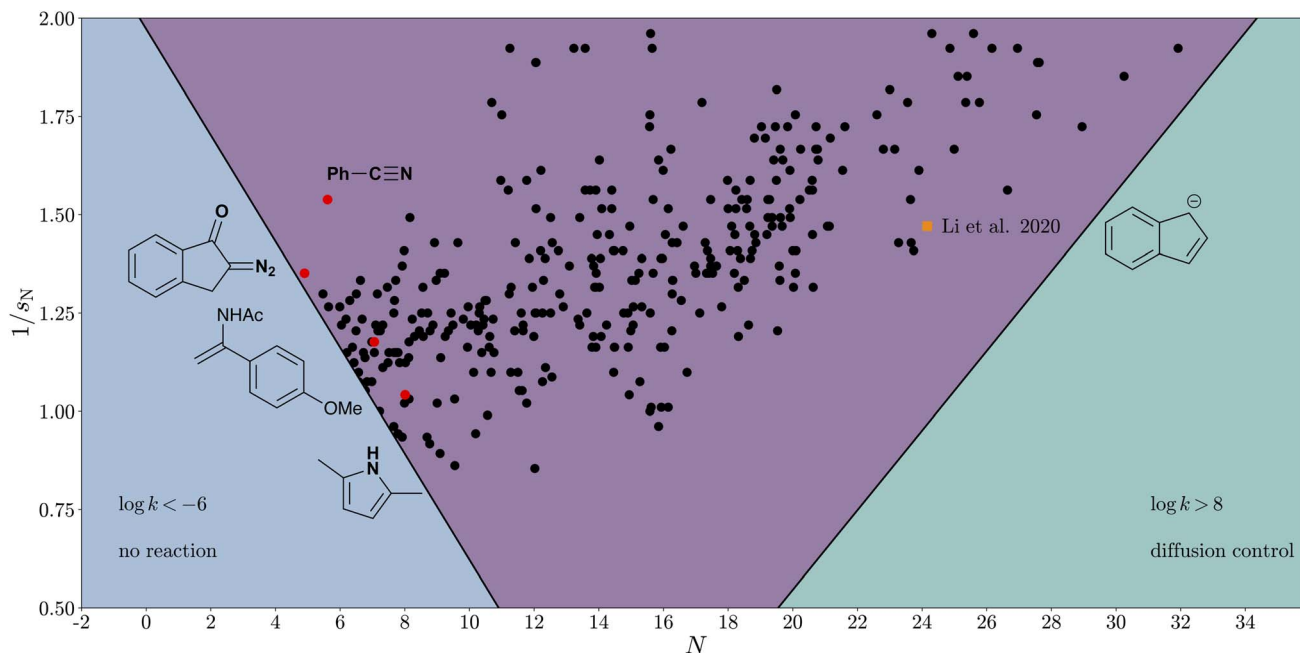
Fig. 7 Reactivity cone for reactions of nucleophiles with CO_2 according to the general Mayr–Patz equation (eqn (9)). Reactivity parameters for CO_2 are set to $s_E = 0.81$ and $E(CO_2) = -14.6$. Here, all carbon-centered nucleophiles of Mayr's database falling into the cone are shown.

To resolve this issue, we developed and trained a multivariate linear (ML) model on experimental data for 20 hetero-allene–carbanion reactions to improve the accuracy of computed rate constants by one order of magnitude compared to the *ab initio* protocol. Both quantum chemical and empirical reactivity information serves as input to the ML model.

ML-predicted rate constants for 15 CO_2–carbanion reactions were subjected to nonlinear least-squares optimisation combined with Bayesian bootstrapping to quantify E for carbon dioxide, $E(CO_2) = -14.6(5)$, with 95% confidence. In contrast to other heteroallenes, it was necessary to relax the otherwise fixed electrophile-specific parameter s_E (default value of 1), which is also done to describe electrophiles undergoing s_N2 reactions.[81] Here, $s_E(CO_2) = 0.81(6)$. A positive implication of an s_E parameter smaller than one is that it expands the substrate scope towards less reactive nucleophiles.

Through these insights, we have gained a refined understanding of the characteristics of CO_2, which helps to better exploit its potential in synthetic and related applications. For example, nucleophiles located within the "CO_2 reactivity cone" developed in this study (Fig. 7) are generally kinetically suitable for undergoing reactions with CO_2 without additional support by transition metal catalysts, Lewis acids, or other activating media. To broaden the scope of application beyond nucleophiles that have been already characterised experimentally, web prediction tools of chemical reactivity can be utilised.[31,34] Identifying new nucleophiles that can successfully undergo carboxylation creates opportunities for designing novel prodrugs or carbamates, thereby enhancing pharmaceutical development or CO_2-binding strategies.

These applications underscore the need to bridge predictions with experimental validation to ensure their practical relevance. Despite the evidence provided by our computational

method, further experiments are unavoidable to truly unveil the reactivity and full potential of CO_2, as well as to clarify the origins of the electrophile-specific parameter s_E.

Data availability

Data for this article, including optimised structures and exemplary input files for quantum chemical calculations are available at **https://doi.org/10.5281/zenodo.14677023**. The data analysis scripts of this article are available in the interactive notebook E_CO2_determination_workflow.ipynb in the same repository.

Author contributions

ME: conceptualization, data curation, formal analysis, investigation, methodology, software, validation, visualisation, writing – original draft preparation, writing – review & editing. KLB: investigation, validation, visualisation, writing – original draft preparation, writing – review & editing. JP: conceptualization, project administration, resources, supervision, writing – original draft preparation, writing – review & editing.

Conflicts of interest

There are no conflicts to declare.

Acknowledgements

References

1 X.-F. Liu, K. Zhang, L. Tao, X.-B. Lu and W.-Z. Zhang, *Green Chem. Eng.*, 2022, **3**, 125–137.

2 S. Dabral and T. Schaub, *Adv. Synth. Catal.*, 2019, **361**, 223–246.

3 J. Artz, T. E. Müller, K. Thenert, J. Kleinekorte, R. Meys, A. Sternberg, A. Bardow and W. Leitner, *Chem. Rev.*, 2018, **118**, 434–504.

4 Q. Liu, L. Wu, R. Jackstell and M. Beller, *Nat. Commun.*, 2015, **6**, 5933.

5 G. Fiorani, W. Guo and A. W. Kleij, *Green Chem.*, 2015, **17**, 1375–1389.

6 C. Das Neves Gomes, O. Jacquet, C. Villiers, P. Thuéry, M. Ephritikhine and T. Cantat, *Angew. Chem.*, 2012, **124**, 191–194.

7 H. Maag, *Prodrugs*, Springer, New York (NY), United States, 2007, vol. 5, pp. 703–729.

8 L. Wang, C. Qi, W. Xiong and H. Jiang, *Chin. J. Catal.*, 2022, **43**, 1598–1617.

9 A. Demessence, D. M. D'Alessandro, M. L. Foo and J. R. Long, *J. Am. Chem. Soc.*, 2009, **131**, 8784–8786.

10 A. C. Forse and P. J. Milner, *Chem. Sci.*, 2021, **12**, 508–516.

11 D.-H. Nam, O. Shekhah, G. Lee, A. Mallick, H. Jiang, F. Li, B. Chen, J. Wicks, M. Eddaoudi and E. H. Sargent, *J. Am. Chem. Soc.*, 2020, **142**, 21513–21521.

12 I. Sullivan, A. Goryachev, I. A. Digdaya, X. Li, H. A. Atwater, D. A. Vermaas and C. Xiang, *Nat. Catal.*, 2021, **4**, 952–958.

13 J. Hong, M. Li, J. Zhang, B. Sun and F. Mo, *ChemSusChem*, 2019, **12**, 6–39.

14 J. Luo and I. Larrosa, *ChemSusChem*, 2017, **10**, 3317–3332.

15 I. I. F. Boogaerts and S. P. Nolan, *J. Am. Chem. Soc.*, 2010, **132**, 8858–8859.

16 I. I. F. Boogaerts, G. C. Fortman, M. R. L. Furst, C. S. J. Cazin and S. P. Nolan, *Angew. Chem., Int. Ed.*, 2010, **49**, 8674–8677.

17 H. Inomata, K. Ogata, S.-I. Fukuzawa and Z. Hou, *Org. Lett.*, 2012, **14**, 3986–3989.

18 Y. Luo and W. Huang, *Org. Biomol. Chem.*, 2023, **21**, 8628–8641.

19 O. Vechorkin, N. Hirt and X. Hu, *Org. Lett.*, 2010, **12**, 3567–3569.

20 S. Fenner and L. Ackermann, *Green Chem.*, 2016, **18**, 3804–3807.

21 S. Felten, C. Q. He, M. Weisel, M. Shevlin and M. H. Emmert, *J. Am. Chem. Soc.*, 2022, **144**, 23115–23126.

22 S. Naumann, *Chem. Commun.*, 2019, **55**, 11658–11670.

23 B. R. Van Ausdall, J. L. Glass, K. M. Wiggins, A. M. Aarif and J. Louie, *J. Org. Chem.*, 2009, **74**, 7935–7942.

24 L. Yang and H. Wang, *ChemSusChem*, 2014, **7**, 962–998.

25 A. Katharina Reitz, Q. Sun, R. Wilhelm and D. Kuckling, *J. Polym. Sci., Part A: Polym. Chem.*, 2017, **55**, 820–829.

26 H. Mayr and M. Patz, *Angew. Chem., Int. Ed.*, 1994, **33**, 938–957.

27 H. Mayr, T. Bug, M. F. Gotta, N. Hering, B. Irrgang, B. Janker, B. Kempf, R. Loos, A. R. Ofial, G. Remennikov and H. Schimmel, *J. Am. Chem. Soc.*, 2001, **123**, 9500–9512.

28 J. Ammer, C. Nolte and H. Mayr, *J. Am. Chem. Soc.*, 2012, **134**, 13902–13911.

29 Z. Li, R. J. Mayer, A. R. Ofial and H. Mayr, *J. Am. Chem. Soc.*, 2020, **142**, 8383–8402.

30 C. Nicoletti, M. Orlandi, L. Dell'Amico and A. Sartorel, *Sustain. Energy Fuels*, 2024, **8**, 5050–5057.

31 Y. Liu, Q. Yang, J. Cheng, L. Zhang, S. Luo and J.-P. Cheng, *ChemPhysChem*, 2023, e202300162.

32 H. Mayr and A. R. Ofial, Mayr's Database of Reactivity Parameters, **https://www.cup.lmu.de/oc/mayr/ reaktionsdatenbank2/**, last accessed on 07 November 2024.

33 H. Mayr and A. R. Ofial, *SAR QSAR Environ. Res.*, 2015, **26**, 619–646.

34 N. Ree, A. H. Göller and J. H. Jensen, *Digit. Discov.*, 2024, **3**, 347–354.

35 N. Ree, J. M. Wollschläger, A. H. Göller and J. H. Jensen, *Atom-Based Machine Learning for Estimating Nucleophilicity and Electrophilicity with Applications to Retrosynthesis and Chemical Stability*, 2024.

36 J. Proppe and J. Kircher, *ChemPhysChem*, 2022, **23**, e202200061.

37 D. B. Rubin, *Ann. Stat.*, 1981, **9**, 130–134.

38 S. Grimme, *J. Chem. Theory Comput.*, 2019, **15**, 2847–2862.

39 P. Pracht, F. Bohle and S. Grimme, *Phys. Chem. Chem. Phys.*, 2020, **22**, 7169–7192.

40 C. Bannwarth, S. Ehlert and S. Grimme, *J. Chem. Theory Comput.*, 2019, **15**, 1652–1671.

41 M. J. Frisch, G. W. Trucks, H. B. Schlegel, G. E. Scuseria, M. A. Robb, J. R. Cheeseman, G. Scalmani, V. Barone, G. A. Petersson, H. Nakatsuji, X. Li, M. Caricato, A. V. Marenich, J. Bloino, B. G. Janesko, R. Gomperts, B. Mennucci, H. P. Hratchian, J. V. Ortiz, A. F. Izmaylov, J. L. Sonnenberg, D. Williams-Young, F. Ding, F. Lipparini, F. Egidi, J. Goings, B. Peng, A. Petrone, T. Henderson, D. Ranasinghe, V. G. Zakrzewski, J. Gao, N. Rega, G. Zheng, W. Liang, M. Hada, M. Ehara, K. Toyota, R. Fukuda, J. Hasegawa, M. Ishida, T. Nakajima, Y. Honda, O. Kitao, H. Nakai, T. Vreven, K. Throssell, J. A. Montgomery Jr, J. E. Peralta, F. Ogliaro, M. J. Bearpark, J. J. Heyd, E. N. Brothers, K. N. Kudin, V. N. Staroverov, T. A. Keith, R. Kobayashi, J. Normand, K. Raghavachari, A. P. Rendell, J. C. Burant, S. S. Iyengar, J. Tomasi, M. Cossi, J. M. Millam, M. Klene, C. Adamo, R. Cammi, J. W. Ochterski, R. L. Martin, K. Morokuma, O. Farkas, J. B. Foresman and D. J. Fox, *Gaussian 16 Revision C.01*, Gaussian Inc., Wallingford (CT), United States, 2016.

42 A. D. Becke, *J. Chem. Phys.*, 1993, **98**, 5648–5652.

43 P. J. Stephens, F. J. Devlin, C. F. Chabalowski and M. J. Frisch, *J. Phys. Chem.*, 1994, **98**, 11623–11627.

44 S. Grimme, J. Antony, S. Ehrlich and H. Krieg, *J. Chem. Phys.*, 2010, **132**, 154104.

45 S. Grimme, S. Ehrlich and L. Goerigk, *J. Comput. Chem.*, 2011, **32**, 1456–1465.

46 F. Weigend and R. Ahlrichs, *Phys. Chem. Chem. Phys.*, 2005, **7**, 3297–3305.

47 F. Weigend, *Phys. Chem. Chem. Phys.*, 2006, **8**, 1057–1065.

48 D. Rappoport and F. Furche, *J. Chem. Phys.*, 2010, **133**, 134105.

49 B. P. Pritchard, D. Altarawy, B. Didier, T. D. Gibson and T. L. Windus, *J. Chem. Inf. Model.*, 2019, **59**, 4814–4820.

50 G. Luchini, J. V. Alegre-Requena, I. Funes-Ardoiz and R. S. Paton, *F1000Research*, 2020, **9**, 291.

51 S. Grimme, *Chem.–Eur. J.*, 2012, **18**, 9955–9964.

52 C. Peng and H. Bernhard Schlegel, *Isr. J. Chem.*, 1993, **33**, 449–454.

53 H. B. Schlegel, *J. Comput. Chem.*, 1982, **3**, 214–218.

54 A. V. Marenich, C. J. Cramer and D. G. Truhlar, *J. Phys. Chem. B*, 2009, **113**, 6378–6396.

55 F. Neese, *Wiley Interdiscip. Rev.: Comput. Mol. Sci.*, 2012, **2**, 73–78.

56 F. Neese, *Wiley Interdiscip. Rev. Comput. Mol. Sci.*, 2022, **12**, e1606.

57 S. Grimme and M. Steinmetz, *Phys. Chem. Chem. Phys.*, 2013, **15**, 16031–16042.

58 P. Pinski, C. Riplinger, E. F. Valeev and F. Neese, *J. Chem. Phys.*, 2015, **143**, 034108.

59 C. Riplinger, B. Sandhoefer, A. Hansen and F. Neese, *J. Chem. Phys.*, 2013, **139**, 134101.

60 C. Riplinger and F. Neese, *J. Chem. Phys.*, 2013, **138**, 034106.

61 T. H. Dunning, *J. Chem. Phys.*, 1989, **90**, 1007–1023.

62 R. A. Kendall, T. H. Dunning and R. J. Harrison, *J. Chem. Phys.*, 1992, **96**, 6796–6806.

63 F. Weigend, A. Köhn and C. Hättig, *J. Chem. Phys.*, 2002, **116**, 3175–3183.

64 C. Hättig, *Phys. Chem. Chem. Phys.*, 2005, **7**, 59–66.

65 A. Halkier, T. Helgaker, P. Jørgensen, W. Klopper, H. Koch, J. Olsen and A. K. Wilson, *Chem. Phys. Lett.*, 1998, **286**, 243–252.

66 A. Halkier, T. Helgaker, P. Jørgensen, W. Klopper and J. Olsen, *Chem. Phys. Lett.*, 1999, **302**, 437–446.

67 M. Eckhoff, K. L. Bublitz and J. Proppe, Determination of the electrophilicity of CO_2, **https://git.rz.tu-bs.de/proppe-group/co2_electrophilicity**, last accessed on 18 November 2024.

68 C. M. Bishop, *Pattern Recognition and Machine Learning*, Springer, New York (NY), United States, 2006.

69 F. Pedregosa, G. Varoquaux, A. Gramfort, V. Michel, B. Thirion, O. Grisel, M. Blondel, P. Prettenhofer, R. Weiss, V. Dubourg, J. Vanderplas, A. Passos, D. Cournapeau, M. Brucher, M. Perrot and É. Duchesnay, *J. Mach. Learn. Res.*, 2011, **12**, 2825–2830.

70 D. J. Wales and J. P. K. Doye, *J. Phys. Chem. A*, 1997, **101**, 5111–5116.

71 P. Virtanen, R. Gommers, T. E. Oliphant, M. Haberland, T. Reddy, D. Cournapeau, E. Burovski, P. Peterson, W. Weckesser, J. Bright, S. J. van der Walt, M. Brett, J. Wilson, K. J. Millman, N. Mayorov, A. R. J. Nelson, E. Jones, R. Kern, E. Larson, C. J. Carey, İ. Polat, Y. Feng, E. W. Moore, J. VanderPlas, D. Laxalde, J. Perktold, R. Cimrman, I. Henriksen, E. A. Quintero, C. R. Harris, A. M. Archibald, A. H. Ribeiro, F. Pedregosa and P. van Mulbregt, *Nat. Methods*, 2020, **17**, 261–272.

72 M. Vahl and J. Proppe, *Phys. Chem. Chem. Phys.*, 2023, **25**, 2717–2728.

73 G. Hoffmann, M. Balcilar, V. Tognetti, P. Héroux, B. Gaüzère, S. Adam and L. Joubert, *J. Comput. Chem.*, 2020, **41**, 2124–2136.

74 M. Eckhoff, J. V. Diedrich, M. Mücke and J. Proppe, *J. Phys. Chem. A*, 2024, **128**, 343–354.

75 P. Pérez, A. Toro-Labbé, A. Aizman and R. Contreras, *J. Org. Chem.*, 2002, **67**, 4747–4752.

76 P. K. Chattaraj, U. Sarkar and D. R. Roy, *Chem. Rev.*, 2006, **106**, 2065–2091.

77 R. S. Mulliken, *J. Chem. Phys.*, 1934, **2**, 782–793.

78 R. G. Parr, R. A. Donnelly, M. Levy and W. E. Palke, *J. Chem. Phys.*, 1978, **68**, 3801–3807.

79 J. Durbin and G. S. Watson, *Biometrika*, 1950, **37**, 409–428.

80 J. Durbin and G. S. Watson, *Biometrika*, 1951, **38**, 159–178.

81 H. Mayr, *Tetrahedron*, 2015, **71**, 5095–5111.

82 C. Schindele, K. N. Houk and H. Mayr, *J. Am. Chem. Soc.*, 2002, **124**, 11208–11214.